

# Resolving Key Questions in Extragalactic Jet Physics

## Abstract

We propose to image a carefully selected sample of bright, extragalactic radio sources with e-MERLIN at L and C bands to provide a legacy data set for jet physics. It is now well established that jets, on all scales, are a key astrophysical phenomenon, and in addition they provide a mechanism for coupling the output of AGN to their large-scale surroundings. Our overarching aim is to measure the physical properties of extragalactic jets: these are key ingredients in understanding the rôle of radio sources in the evolution of structure in the Universe and the production of high-energy cosmic rays. Our primary science questions include:

1. What are the dynamics of radio jets in the vicinity of the AGN? How are low-luminosity radio jets decelerated on sub-kpc scales? What are the jet velocities, magnetic-field structures, powers, mass fluxes and entrainment rates? The key new aspect of the e-MERLIN observations is the ability to resolve the jets where they first brighten.
2. What are the three-dimensional structures of powerful jets? Do they have highly relativistic “spines”? e-MERLIN will allow transverse resolution of the jets with good sensitivity for the first time.
3. What are the magnetic field configurations immediately surrounding jets? Is there evidence for confining fields? e-MERLIN will be able to determine Faraday rotation measures within a single observing band at high spatial resolution.
4. Where and how are particles accelerated in the hot-spots and jets of powerful sources? By allowing us to measure synchrotron spectra and polarization in many discrete regions across these kpc-scale regions, e-MERLIN will enable studies of their electron populations and magnetic field sub-structures.

We will select the brightest few representative examples of distinct types of source from well-defined samples limited by flux density and redshift and observe them with high sensitivity and image fidelity. Our targets are the defining members of their classes, and include famous objects such as Cygnus A, M 87 and 3C 273. Without exception, they have a wealth of data available at radio and other wavelengths, and the new observations will have enduring legacy value.

We propose 20 full tracks (339 hr) at C-band and 22 tracks (390 hr) at L-band, using the maximum possible bandwidth in full polarization.

## Team members

P. Alexander	Cavendish Laboratory, Cambridge	S. Garrington	JBCA, University of Manchester
M. Birkinshaw	University of Bristol	D. Guidetti	INAF - IRA, Bologna/ESO
A.H. Bridle	NRAO	M.J. Hardcastle	University of Hertfordshire
I.W.A. Browne	JBCA, University of Manchester	R.A. Laing	ESO
W.D. Cotton	NRAO	J.P. Leahy	JBCA, University of Manchester
J.H. Croston	University of Hertfordshire	R. Morganti	ASTRON
F. Dulwich	University of Oxford	P. Parma	INAF - IRA, Bologna
D.A. Evans	Harvard/CfA	J.M. Riley	Cavendish Laboratory, Cambridge
D. Gabuzda	University College Cork	D.M. Worrall	University of Bristol

Coordinator: R.A. Laing

ESO, Karl-Schwarzschild-StraÙe 2, D-85748 Garching-bei-München, Germany

rlaing@eso.org

# 1 Introduction: jets in context

## 1.1 Jets

Jets – fast, highly-collimated, bipolar outflows – are inextricably linked to the processes of accretion and collapse onto compact astrophysical objects. They are observed in Young Stellar Objects, microquasars, pulsar wind nebulae,  $\gamma$ -ray burst sources and, most spectacularly, in the objects that are the subject of this proposal, radio galaxies. Not only can these jets be the primary channel of energy loss from accreting supermassive black holes (SMBH), but they also have a major impact on their surroundings, and related particle acceleration produces the most energetic photons and hadrons we observe. The quantitative study of relativistic jets is notoriously difficult, because they emit primarily by the broad-band synchrotron and inverse Compton processes which offer few diagnostics of physical parameters. Major progress in understanding jet physics on large scales has recently come from the combination of detailed radio observations with data at other wavebands, particularly X-ray imaging and spectroscopy. The purpose of the present proposal is to extend these techniques to smaller angular scales, where only e-MERLIN can provide adequate spatial resolution and sensitivity.

## 1.2 Feedback, structure formation and black-hole growth

Many of the issues in understanding the structures of galaxies, groups of galaxies, and clusters of galaxies are thought to be resolved by suitably-tuned feedback of energy and momentum from dense to diffuse phases of matter. Such feedback is believed to be necessary to account for the properties of the structures that we see today, and to be responsible for the tight relationships between galaxy bulge and central SMBH masses. Although starbursts and Seyfert nuclei may have some effect, radio galaxies are thought to provide the strongest feedback and therefore to affect structure formation on the largest range of mass scales: quantitative estimates based on the energetics of cavities in dense X-ray emitting gas show that the energy provided by radio galaxies can easily reverse gas infalls on scales of hundreds of kpc. Although ample energy input is available from jets, neither the way in which feedback is regulated nor the processes which heat the intergalactic medium are currently understood. To resolve the latter issue, we need to quantify the mass, momentum and energy inputs from jets and to work out how they interact with their surroundings.

## 1.3 Jets as particle accelerators

Extragalactic relativistic jets generate the most energetic photons we observe:  $\gamma$ -rays with energies 1 – 10 TeV

(now detected from tens of sources with jets pointing nearly towards us and from the nearby radio galaxy M 87). Recent results from the Auger Observatory (Abraham et al. 2007) suggest that the highest-energy cosmic rays, with energies in excess of  $6 \times 10^{19}$  eV, originate in AGN. An excess centred on Centaurus A suggests that some at least may be accelerated in radio galaxies. At lower energies (below the GZK cutoff) radio-loud AGN plausibly provide the bulk of the high-energy cosmic ray population. Although it has been known for many years that various components of radio galaxies are in principle capable of high-energy cosmic ray acceleration (Hillas 1984), there is no consensus on the location of the acceleration sites or the underlying physical mechanisms. We cannot observe the most energetic electrons directly in the radio band, but the combination of high-resolution radio, optical and X-ray imaging provides our most detailed picture of acceleration at work. It has become clear that simple, spatially-homogeneous acceleration models are inadequate, and that there is probably more than one acceleration process at work in the same physical volume. Interpretation depends critically on accurate spectral measurements with high spatial resolution in jets and their terminal hot-spots.

## 1.4 An approach to jet physics: working from large to small scales

Relativistic jet formation occurs on scales  $\lesssim 100 R_G$  ( $\lesssim 1$  milliarcsec), so direct study of this process is only possible with VLBI techniques, supplemented by coordinated observations of time variability across the electromagnetic spectrum. Why, then, is e-MERLIN so important? The principal reason is that a detailed understanding of jet flows – compositions, velocity fields, energetics, acceleration physics, magnetic fields and interactions with the environment – can only be gained from *deep, transverse-resolved* radio observations. Until now, these have only been feasible on  $\gtrsim 0.25$ -arcsec scales with the VLA. We want to take the next steps: inwards towards the nucleus and outwards to the regions where the jets impact on their surroundings, capitalising on the improvements in sensitivity and resolution that only e-MERLIN can provide.

Our scientific questions are:

1. What are the velocity fields, mass, energy and momentum fluxes in jets? Do powerful jets have highly relativistic spines and, therefore, are beamed inverse Compton models for kpc-scale jet X-ray emission viable? How do jet energy fluxes compare with estimates from cavity dynamics? How and where do jets interact with the external medium? What is the relative importance of mass input from stars in the jet volume and boundary-layer ingestion?

2. In what form is the energy carried: leptons, baryons or electromagnetic? Are constraints on the mass flux sufficient to rule out models in which most of the kinetic energy is carried by protons? Conversely, do we see evidence for electron acceleration mechanisms which require cold protons? What are the three-dimensional magnetic-field structures in and around jets, as inferred from synchrotron emission and Faraday rotation, respectively? Can we find evidence for magnetic confinement of jets?
3. Where are the main sites of high-energy particle acceleration? Is there morphological or spectral evidence for more than one acceleration mechanism at work in the same region? If so, are the relative efficiencies related to jet speed, velocity shear or the presence of shocks? What causes the apparently universal spectral behaviour in low-luminosity jet bases?

We will address these questions using e-MERLIN studies of several different classes of radio-loud AGN.

## 2 Scientific Justification

### 2.1 Low-luminosity jets: the physics of deceleration

#### 2.1.1 Jets on kiloparsec scales

The division of radio galaxies into two morphological classes by Fanaroff & Riley (1974) has proved to be remarkably robust. FRI sources are centre-brightened and have low radio luminosities; FR II sources are edge-brightened and luminous. The division between the two classes corresponds to a radio luminosity of  $P_{1.4\text{GHz}} \approx 2 \times 10^{25} \text{ W Hz}^{-1}$ ; there is also a strong dependence on the stellar luminosity of the host galaxy (Ledlow & Owen 1996)<sup>1</sup>. It is now accepted that the jets in FRI sources decelerate from relativistic to sub-relativistic speeds on kiloparsec scales, flaring and radiating as they do so. We have quantified the physics of jet deceleration in FRI radio galaxies using deep VLA observations, X-ray imaging and sophisticated models (e.g. Laing & Bridle 2002a; Laing et al. 2006b). Our modelling has enabled us for the first time to estimate the variations of velocity, magnetic-field structure and proper emissivity of FRI jets in three dimensions as well as their intrinsic geometries and orientations. We assume that the jets are intrinsically symmetrical and relativistic, so apparent differences between them (in both brightness and linear polarization) result from special relativistic aberration. We calculate the emission from a model jet in Stokes  $I$ ,  $Q$  and  $U$  by numerical integration, accounting for relativistic aberration and anisotropic

<sup>1</sup>We assume a cosmology with a Hubble constant  $H_0 = 70 \text{ km s}^{-1} \text{ Mpc}^{-1}$ ,  $\Omega_\Lambda = 0.7$  and  $\Omega_M = 0.3$ .

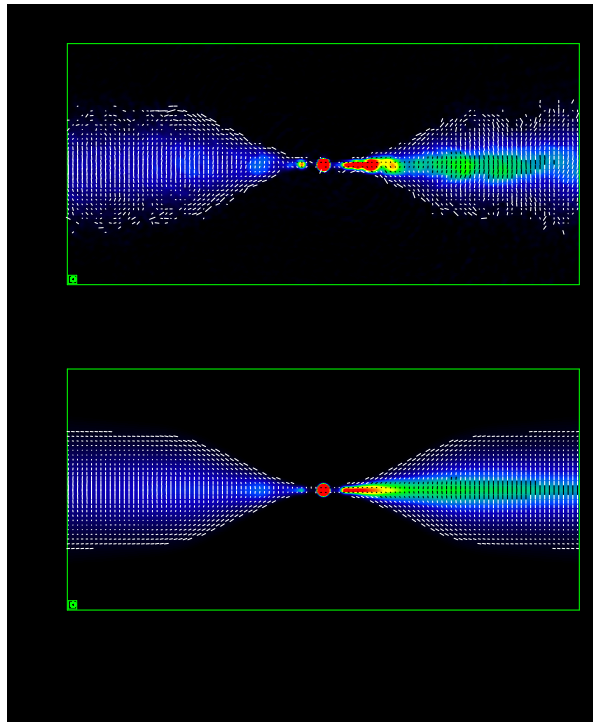


Figure 1: A comparison between data (top) and model (bottom) for the inner jets of the FRI radio galaxy 3C 296 Laing et al. (2006b). The total intensity is in false colour; the vector lengths are proportional to the degree of polarization and their directions are along the apparent magnetic field. The image extends  $\pm 40$  arcsec from the nucleus.

rest-frame emission, and convolve to the resolution of our VLA images. We then optimize the model parameters. An example fit is shown in Fig. 1. We find that all of the jets have inferred bulk Lorentz factors  $\Gamma \approx 2$  where they first brighten appreciably. In the flaring regions, all of the modelled jets decelerate abruptly, thereafter either maintaining a much slower, constant (but still mildly relativistic) speed or slowing less rapidly. The jets also show transverse velocity gradients, with edges roughly 30% slower than the centres in all but one case. The three-dimensional structure of the magnetic field is mainly a mixture of toroidal and longitudinal components, the former dominating at large distances from the nucleus.

These FRI jets must decelerate by entrainment. A conservation-law analysis incorporating external pressure and density profiles from X-ray observations (Laing & Bridle 2002b) gives the variation of internal pressure, density, Mach number and entrainment rate along the jets, together with estimates of energy and mass fluxes. The derived energy fluxes ( $10^{36} - 10^{37} \text{ W}$ ) are directly comparable with estimates of the work required to inflate X-ray cavities, if these can be observed. Where the jets brighten abruptly, they must be overpressured with respect to their surroundings, driving the observed rapid expansion. They are light, with densities on kiloparsec scales roughly equivalent to only one proton  $\text{m}^{-3}$ . The initial deceleration requires an entrainment rate which is

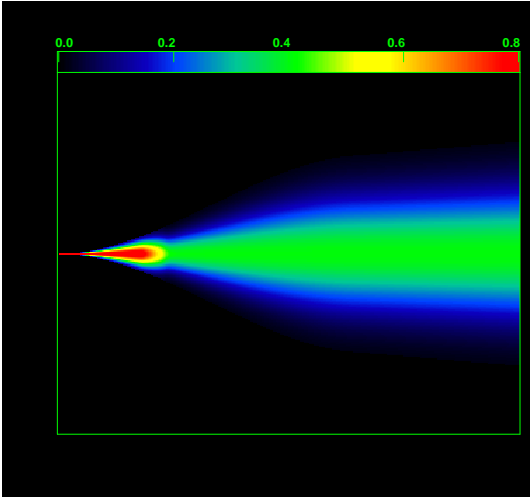


Figure 2: The velocity field (in units of  $c$ ) derived for the jets in 3C 296 from the model fits in Fig. 1

remarkably close to that predicted from mass loss by stars within the jet volume. There is evidence in at least one case for additional mass input, presumably via boundary-layer entrainment, but it is plausible that essentially all of the jet mass at 1 kpc comes from stars inside the jet volume, consistent with an electron-positron or electromagnetic jet on small scales.

### 2.1.2 What initiates deceleration?

A key question left unanswered by these studies is *what initiates the brightening, flaring and deceleration of FRI jets?* The characteristic structure of an FRI jet base is a faint, well-collimated inner region followed by sudden brightening and flaring as in Fig. 3 (Worrall et al. 2007). Our VLA observations usually resolve the jets transversely only after they brighten, and our modelling technique constrains the jet velocity only at larger distances. One possibility is that the inner jets decelerate abruptly at standing (e.g. reconfinement) shocks and thereafter interact violently with the surrounding medium. A second is that the initial expansion results from the rapid decrease of external pressure inferred from X-ray observations (in which case the jets may even *accelerate*), after which there is progressively increasing mass loading both from stars inside the jet volume and/or boundary-layer entrainment. e-MERLIN at L-band provides precisely the right resolution to image the start of the flaring region in detail. All of the jets we have observed in detail show complex, non-axisymmetric fine structure after they flare. Thus far, the best-resolved example is NGC 315 (Fig. 3), where the angular size is large enough to show some detail at 0.4-arcsec resolution and the fine structure looks like a helical filament. e-MERLIN observations at 0.1-arcsec resolution will allow us to answer the following questions:

1. Is there morphological evidence for shocks where

the jets first brighten? Does the non-axisymmetric, knotty structure after the brightening point have a characteristic form?

2. What is the velocity field close to (and, in the brighter cases, before) the brightening point? Is there any evidence for fast flow close to the jet axis? Do the jets decelerate suddenly as they brighten or even accelerate due to the action of an external pressure gradient? We can apply our jet models to fit the e-MERLIN data simultaneously with our existing VLA observations to get a clear picture of the jet kinematics in these regions.
3. Does the magnetic-field structure of the inner jets differ from that further out? Can we detect any evidence for systematic gradients in Faraday rotation measure associated with a collimating magnetic field in the surrounding thermal plasma (cf. Section 2.2.4) or interactions with the surrounding IGM?
4. Are there any spectral gradients across the structure? Synchrotron X-rays are produced in these regions, so a particle-acceleration mechanism is definitely required. We have shown that a characteristic spectral index of  $\alpha = 0.61$  ( $S \propto \nu^{-\alpha}$ ) is associated with FRI jet bases where they first brighten and that there is evidence for spectral flattening associated with shear at larger distances (Laing et al. 2006a), but the spectra of the faint inner jets are not well-determined. Can we find signatures associated with the cyclotron instability, which has recently been suggested as the cause of the universal break in the spectrum of FRI jets at electron Lorentz factors  $\gamma \sim m_p/m_e$ ? If so, the jet kinetic energy must be dominated by cold protons (Amato & Arons 2006).
5. Can we determine consistent conservation-law solutions from 100 pc –  $\gtrsim$  10 kpc from the nucleus? Are the mass fluxes we infer on the smallest scales low enough to rule out a significant proton component in the inner jets? Could they plausibly arise entirely from stellar mass loss within the jet volume, as estimated from HST light profiles? What are the energy fluxes and how do they compare with values determined from X-ray cavity dynamics?

In order to answer these questions, we propose to observe a sample of twin-jet FRI sources, selected to have jets bright enough to image with good signal-to-noise at L-band (Section 3.2 and Appendix A). As we are observing two-sided jets from a flux-limited parent sample selected at low frequency, Doppler favouritism does not introduce significant selection biases: we are targeting the brightest and closest examples in order to maximise the signal-to-noise ratio and linear resolution.

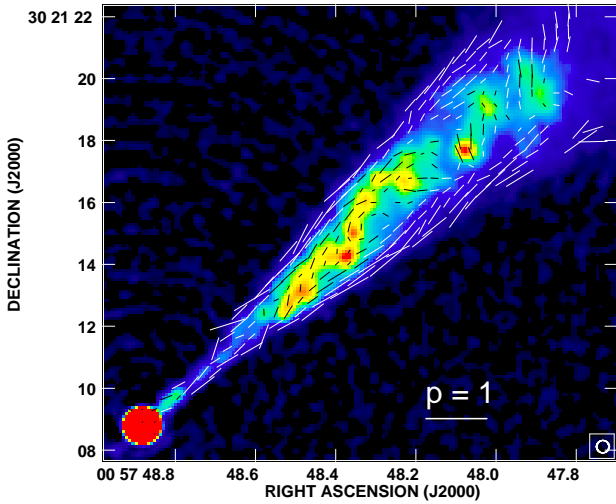


Figure 3: The inner jet of NGC 315, as observed with the VLA at a resolution of 0.4 arcsec (Worrall et al. 2007).

We will analyse the resulting images using our well-tested codes for modelling jet kinematics and rotation-measure fluctuations. The kinematic models will, in turn, provide the geometry and velocity profiles required for conservation-law analyses, leading to energy, mass and momentum flux estimates.

### 2.1.3 Proper-motion measurements: direct velocity estimates in M 87

A complementary approach to estimates of jet flow speeds through modelling of asymmetries is the direct measurement of proper motions. This is only possible in the nearest radio galaxies with bright substructure in their jets: M 87 (Biretta, Zhou & Owen 1995; Biretta, Sparks & Macchetto 1999) and Cen A (Hardcastle et al. 2003, too far South for e-MERLIN). M 87 shows a complex pattern of outward motions with apparent speeds up to  $\approx 6c$  and flux changes, for example in the highly-variable HST-1 complex close to the nucleus (Cheung, Harris & Stawarz 2007). The high resolution (0.04 arcsec) and good spatial-frequency coverage of e-MERLIN at C-band will allow a significant improvement on the 0.1-arcsec 15-GHz VLA observations of Biretta, Zhou & Owen (1995) and a direct comparison with HST imaging. We aim to answer the following questions:

1. We know that there are significant differences in the locations of radio, optical and X-ray emission in the M 87 jet (e.g. Marshall et al. 2002): are there also differences in the apparent speeds? Is there evidence for velocity stratification?
2. Are the highest velocities indicative of the underlying flow, or are they best interpreted as pattern speeds?

3. Is there a sudden deceleration in the flow at knot A, as implied by lower-resolution data (Biretta, Zhou & Owen 1995); if so, is this analogous to the flaring points in other FR I jets (cf. Section 2.1.2)?
4. What is the distribution of optical-radio spectral index at high spatial resolution? Is there evidence for different acceleration mechanisms for the small-scale structure, the apparent shock front in knot A or the diffuse emission?

We propose 5 epochs of observation of the M 87 jet at C-band, as discussed in more detail in Section 3.3. In addition, we ask for one track at L-band to image the larger-scale emission.

## 2.2 Powerful jets: highly relativistic flows?

### 2.2.1 The flow-speed problem

We have established rather less about the physical parameters of jets in powerful (predominantly FR II) radio galaxies. It has been known for many years (e.g. Laing 1993) that they must remain at least mildly relativistic until they terminate. There is an ongoing debate on the mechanism of X-ray emission from powerful jets which is closely related to this issue. The two alternatives are:

1. The X-rays observed in the extended jets associated with core-dominated sources are generated by inverse Compton scattering of cosmic microwave background photons by relativistic electrons in the jet. These electrons must therefore have large bulk Lorentz factors  $\Gamma \sim 10$  and the jets must be close to the line of sight (Tavecchio et al. 2000; Celotti et al. 2001).
2. The X-ray and radio emission are both generated by the synchrotron mechanism, but not necessarily from the same electron population.

(see Hardcastle 2006 for a critical review). A necessary consequence of the first (ICMB) hypothesis is that the parent population of the core-dominated sources – FR II sources in general – must also have jets with fast flow speeds. In order to reconcile this with estimates of their velocities from sidedness ratios, typically in the range  $0.6 - 0.7c$  (Wardle & Aaron 1997), it is necessary to postulate that a  $\Gamma \sim 10$  *spine* is surrounded by a  $\Gamma \lesssim 2$  *shear layer* – implying velocity gradients significantly larger than those we find in FR I jets.

### 2.2.2 Measuring the velocity profile

In order to estimate the velocity profiles for FR II jets, we adopt a statistical approach, using e-MERLIN to make the first transverse-resolved observations of one-sided jets over a range of orientations. If velocity structure is present

in jets, then the structures we see in total intensity and polarization will depend strongly on the angle made by the jet to the line of sight. If the jet spine is highly relativistic with Lorentz factor  $\Gamma_{\text{spine}}$ , we expect its emission to be strongly Doppler suppressed for angles to the line of sight  $\theta \gtrsim 1/\Gamma_{\text{spine}}$ . If the rest-frame emission from spine and shear layer are comparable, then the jet would appear limb-brightened, as is indeed the case for the one FR II jet that has been resolved adequately by the VLA, 3C 353 (Swain, Bridle & Baum 1998). For  $\theta \lesssim 1/\Gamma_{\text{spine}}$ , however, the emission from the spine is Doppler boosted and the jet appears centre-brightened. By selecting a sample of objects whose angles to the line of sight span a *wide range* (based on constraints from superluminal motion, where available, and from core and jet prominence and jet sidedness otherwise) we should be able to decouple rest-frame emissivity and Doppler effects. We stress that the sample does not need to have an *unbiased* distribution of orientations.

If  $\Gamma_{\text{spine}} \sim 10$ , as is required by beamed inverse Compton models for X-ray emission from quasar jets, then we expect the spine emission to be significantly enhanced for sources with  $\theta \lesssim 0.1$  rad. We would then need to compare the transverse brightness profiles for core-dominated sources showing extreme superluminal motion with those at more modest inclinations. We have included three sources with extended jets which also show apparent superluminal velocities  $\approx 15c$  on parsec scales, requiring  $\theta \lesssim 4^\circ$  (3C 273, 345 and 454.3). For comparison, we need objects covering a similar range of extended radio luminosity, with jets that are bright (so that we can measure their transverse profiles) and straight (so that the assumption of a single angle to the line of sight is valid). We have chosen extended quasars and broad-line radio galaxies from the LRL sample with  $0.25 \leq z \leq 1$  (e.g. Fig. 4). Unified models suggest that  $\theta \lesssim 50^\circ$  for these sources, and we can derive estimate orientations from a combination of VLBI proper-motion measurements, core and jet prominence. Even with crude binning in  $\theta$  and averaging over intrinsic or environmental asymmetries, our sample size is large enough that we will be able to draw robust conclusions about intensity and therefore velocity profiles. We can also compare our results with observations of the jets in Cygnus A, which is likely to be much closer to the plane of the sky than the rest of sources, but is comparable in extended luminosity. We can observe its jets in detail because it is anomalously close and bright, and it is already part of our hot-spot sample.

Our primary tool for image analysis will be the jet-modelling code described in Section 2.1.1, modified slightly for the different conditions in FR II jets. We expect the observed polarization structure to change significantly as a function of angle due to relativistic aberration; our models use this to constrain both the intrinsic field structure and the jet velocity field. We will analyse variations along as

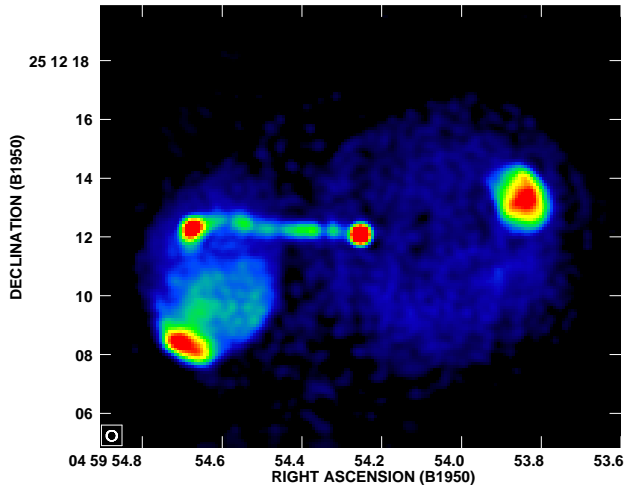


Figure 4: 3C 133, a radio galaxy with a powerful, one-sided jet, observed at a resolution of 0.35 arcsec with the VLA (Floyd et al. 2006).

well as across the jets, since inverse-Compton models also imply jet deceleration in many cases. The spine-sheath model makes a clear *qualitative* prediction of the dependence of jet surface brightness structure on angle to the line of sight, which we will be able to test immediately. If it is verified, we will be able to use the details of the dependence to determine some *quantitative* constraints on jet speed as a function of position in the jets.

### 2.2.3 3C 273: an end-on jet in detail

3C 273 is the best-studied powerful jet and, because of its strong X-ray emission, a key source for detailed tests of the beamed inverse-Compton model (e.g. Jester et al. 2005; Hardcastle 2006). MERLIN observations have already been instrumental in studying the detailed structure of the jet at L-band, where *e-MERLIN sensitivity* is not required. Where we can now do much better is in *image fidelity* and in the ability to measure the wavelength variations of polarization and total intensity at high spatial resolution and with exquisite sensitivity. We will also be able to image the jet at C-band with even higher spatial resolution and therefore to make a fine-scale comparison with the existing *HST* observations, thereby constraining the sites of the particle acceleration responsible for the optical and possibly the X-ray emission. Polarization observations are particularly powerful in separating multiple synchrotron components, as demonstrated at lower resolution for 3C 273 by Uchiyama et al. (2006).

### 2.2.4 Rotation measures and external magnetic fields

While the synchrotron polarization corrected for Faraday rotation is determined by the structure of the magnetic field in the emitting regions, Faraday rotation (quantified by the rotation measure, RM) is produced by magnetic

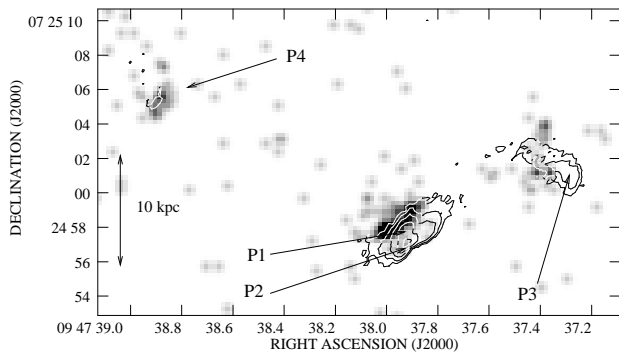


Figure 5: *Chandra* X-ray images (greyscale) overlaid with VLA 8-GHz contours ( $\sim 0.25$ -arcsec resolution) of the W hot-spots of 3C 227 (Hardcastle et al. 2007). A clear offset of a few kpc is seen between the peak of the X-ray and any of the peaks in the radio emission.

field in thermal plasma between us and the emission, almost always in front of the synchrotron emission rather than mixed with it. Gradients of RM are frequently seen across radio sources, but their relationship to the structure is often unclear, because of limited resolution or sensitivity. A systematic change of sign of RM across a jet is a clear signature of jet collimation by toroidal magnetic fields. The wide-band capability of e-MERLIN allows us to determine the variation of RM across a jet at high spatial resolution in a single observation, something which has never been possible previously for powerful jets.

### 2.3 Particle acceleration: hot-spots and jet knots

Where and how are particles accelerated in the hot-spots and jet knots of powerful sources? By allowing us to measure synchrotron spectra and polarization in many discrete regions across these kpc-scale regions, e-MERLIN will enable studies of their electron populations and magnetic field sub-structures.

In the standard picture, the hot-spots of powerful (FR II) radio galaxies and radio-loud quasars are the visible manifestations of strong shocks where the relativistic beams of energetic particles are suddenly decelerated by interaction with the slow-moving or stationary plasma within the radio lobes. The particle acceleration at these shocks determines the energy distribution of the electrons (and, possibly, protons) that go on to form the large-scale lobes and expand into the external medium, and so an understanding of how and where the process happens is essential to an understanding of the dynamics and environmental impact of radio sources. In addition, the strong shocks in FR IIs are often invoked as possible accelerators of high-energy cosmic rays, so it is important to understand where (and if) high-energy particles are accelerated in these systems.

The strongest evidence for the standard model comes from the radio through optical spectra of hot-spots, which have been shown (e.g. Meisenheimer et al. 1989) to be

commonly consistent with the predictions of a simple ‘continuous injection’ model for shock particle acceleration and downstream losses (Heavens & Meisenheimer 1987). However, there are at least three reasons to suppose that this model cannot be right in detail:

1. **Double hot-spots:** It has been known for many years (e.g. Laing 1982) that some sources show more than one feature meeting the definition of a hot-spot in a given lobe. The configuration of the hot-spots relative to the jet flow often suggests that more than one is associated with the beam termination and various models exist to explain their nature. It is now clear that particle acceleration is not restricted to one location in at least some examples (Hardcastle et al. 2007).
2. **Spectral problems:** Optical and, more recently, X-ray data show that in many cases the broad-band spectra of hot-spots do not agree with the ‘continuous injection’ model. The problem is particularly clear in the X-ray where hot-spot spectra are often required to be concave (e.g. Tavecchio et al. 2005; Kraft et al. 2007) implying (in a synchrotron model for the X-rays) multiple electron populations within the large region sampled by the broad-band spectrum.
3. **Spatial offsets:** It has become clear that the high-energy emission from hot-spots often does not even come from the same location as the bulk of the radio emission (Fig. 5). This rules out an inverse-Compton model for the X-rays but requires that the location of the high-energy particle acceleration must be separated from the radio hot-spot by a distance which may be anything between a few kpc (Hardcastle et al. 2002, 2007) and 20 kpc (Erlund et al. 2007). In some cases there is no apparent radio emission associated with the peak in the (clearly extended) X-rays.

In the radio, hot-spots are observed to have sizes of a few kpc, corresponding to at most a few arcsec at the distances of interest (since FR II radio galaxies are comparatively rare and there are no very nearby objects). This has the effect that their detailed radio structures have been relatively poorly studied, despite the high surface brightness observed in many systems. At the VLA one needs to work at high frequencies to obtain the required resolution, with consequent loss of sensitivity, while even at the lowest frequencies hot-spots are typically resolved out by the VLBA. MERLIN has a proven record in hot-spot studies (e.g. Hardcastle et al. 1997; Gilbert et al. 2004; Fig. 6) although its capabilities have been limited by image fidelity and sensitivity problems. e-MERLIN will not have these limitations: in addition, and crucially, we will be able to map the radio *spectrum* across the whole of the hot-spot

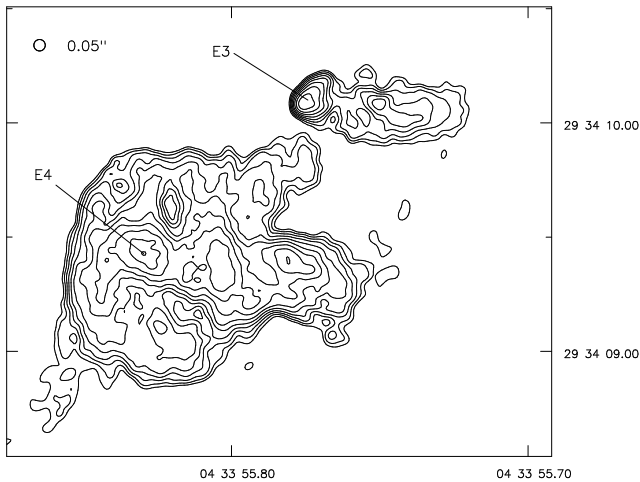


Figure 6: MERLIN 5-GHz image of the E hot-spots of 3C 123 from Hardcastle et al. (1997). At MERLIN’s angular resolution (corresponding to a spatial resolution of 0.2 kpc) a wealth of complex spatial structure is seen which appears entirely inconsistent with a simple model of the hot-spot region as a planar shock with downstream energy losses.

region. To date there has been essentially no capability of studying the variation of radio spectrum as a function of position, even though this provides us with the only tool to understand how the electron energy spectra vary across the region (and even though we know from optical and X-ray work that there clearly *is* strong dependence of the electron spectra on position within the hot-spot). In addition, e-MERLIN observations will allow us to investigate the magnetic field structure of the hot-spots.

The hot-spot observations proposed as part of the legacy project will address the following observational questions:

1. How does the radio spectrum of hot-spots vary as a function of position? How does it relate to the observed optical (especially *HST*) and X-ray emission? Is there evidence for particle acceleration throughout the hot-spot region or is it localized?
2. In hot-spots exhibiting offsets between radio and X-ray peaks, what is the structure and spectrum of radio emission coincident with the X-ray emission?
3. What are the characteristic total intensity and polarization structures in the hot-spots, and how do they relate to the presumed energy supply from the jet? Are all hot-spots appropriately modelled as jet-termination structures? (In this context, numerical simulations by Tregillis et al. 2002 show ‘hot-spots’ that may not be related either to jet termination or to particle acceleration.)
4. In multiple-hot-spot systems, what are the differences in spatial and spectral structures between the hot-spots? Are there any true relic (‘dentist’s drill’)

hot-spots or is multiple hot-spot generation always related to redirection of outflow?

To address these questions, we will observe the brightest hot-spots covering the full range of morphologies and high-energy emission processes, again selected from the orientation-independent LRL sample (see Section 3.5 and Appendix A). All of our target objects have good optical and X-ray coverage. Since most of the hot-spots have surface brightnesses high enough that e-MERLIN will be able to image all their structure even at the full C-band resolution, we primarily work in C-band for this part of the proposal. However, a number of sources have structures large enough that they should be well resolved at L-band (this is particularly true of nearby double-hot-spot sources) and so we will observe these in both bands. This will allow us to broaden the range of our spectral imaging and to image faint structure around the hot-spot regions.

For almost all the hot-spots in the sample, the detailed information on total intensity and magnetic field orientation provided by the new data will provide strong constraints on the jet-hot-spot relationship. e-MERLIN’s capabilities for imaging spectral and rotation measure structure will allow us to relate hot-spot structure respectively to particle acceleration and to external magnetic field configuration. For multiple hot-spots, we will also look at the relationship of hot-spots to each other: is there evidence for continued outflow between hot-spots? For hot-spots with inverse-Compton X-rays, we will use the e-MERLIN data to make detailed inverse-Compton predictions and compare with observations. Where optical or X-ray synchrotron is seen, we will investigate the offsets seen in many of our targets and relate spectral and polarization structure to models of particle acceleration. As each class of hot-spot is represented by several objects in our sample, the end result will be a *general* set of answers to each of the scientific questions posed above.

### 2.3.1 Cygnus A: the nearest powerful radio source

Cygnus A presents a unique opportunity for hot-spot studies. As is well known, it is anomalously luminous (by several orders of magnitude) for its redshift and its hot-spots have the highest flux densities of any in the sky (by more than a factor of ten). This means that their high-resolution structures are already quite well studied (e.g., Dreher 1981) but it also means that e-MERLIN will particularly sensitive to their spectral structure. In addition, Cygnus A’s secondary hot-spots are strong inverse-Compton sources (Harris et al. 1994) and are resolved even with *Chandra*, so that we will be able to use the radio emission to probe structures in the *strength* of the magnetic field in the hot-spot. The results from detailed analysis of the Cyg A hot-spots will feed directly into our studies of other objects in the sample.

### 3 Technical justification

#### 3.1 Sample selection: general principles

Our targets are chosen from well-defined flux-limited samples selected at low frequencies, principally by Laing, Riley & Longair (1983, LRL). The low selection frequency (178 MHz) ensures that the parent sample is not seriously affected by orientation biases. Where the LRL sample contains too few examples of a given type of object, and for a few anomalously bright special cases, we have included sources satisfying the same flux-density limit over larger areas of sky. Imaging of linear polarization, image fidelity and sensitivity are critical to our science case, so we will observe using the maximum available bandwidth in L and C bands, in full polarization. Although the sources are strong, the structures we wish to image are typically heavily resolved by e-MERLIN: except in the brightest cases, we will be limited by the sensitivity required to image linearly polarized emission. We have considered the possibility of observing one sub-band at higher spectral resolution for the nearer targets in order to image HI absorption, but our current view is that this might compromise rotation-measure studies, which benefit from uniform frequency sampling across the band. We will review this decision based on commissioning observations.

We have evaluated the expected surface brightnesses for our targets using the highest-resolution images available (typically from the VLA at 0.25 – 1.0 arcsec FWHM). We assume that the structures we wish to observe (jets and hot-spots) are fully resolved and scale by the ratios of the beam areas, assuming 0.15 arcsec and 0.04 arcsec FWHM for e-MERLIN at L and C-band, respectively, appropriate for natural weighting with the Lovell Telescope included. This gives conservative estimates for the surface brightness if the structure is partially resolved. We also assume that the spectral index is  $\alpha = 0.6$ . We have estimated values for the peak and typical (minimum) surface brightnesses over the regions of interest: these values are necessarily approximate, given the large extrapolation from published data. In practice, we expect to trade off resolution and surface-brightness sensitivity by adjusting the data weighting. Our estimates are given in Appendix A for all of our targets.

Given the combined requirements of sensitivity and image fidelity, we have chosen to propose one full track (defined so that the source elevation is above  $5^\circ$  at all of the sites) for each of our target/frequency combinations. Very roughly, we need to be able to detect linear polarization (typically 10%) at the  $4\sigma$  level. Given rms sensitivities for full tracks  $\approx 2\mu\text{Jy}/\text{beam}$  at C-band and  $\approx 5\mu\text{Jy}/\text{beam}$  at L-band (with the Lovell Telescope in the array), this sets surface-brightness limits in total intensity of  $\approx 80\mu\text{Jy}/\text{beam}$  at C-band and  $\approx 200\mu\text{Jy}/\text{beam}$  at L-band. These numbers are consistent with the conservative

estimates of  $S_{\min}$  given in Appendix A.

For some of the brighter sources, we either do not need the full sensitivity or are likely to be limited by dynamic range. We have indicated in Appendix A those sources which have  $S_{\min} \geq 500\mu\text{Jy}$  at L-band or  $S_{\min} \geq 200\mu\text{Jy}$  at C-band and those where dynamic-range restrictions are likely to preclude reaching the theoretical sensitivity. We propose to observe these with MkII rather than the Lovell Telescope in the array, as shown explicitly in Appendix A.

In all cases, the regions we are interested in imaging with e-MERLIN are far smaller than the primary beam (we quote the relevant scales in Appendix A). Many of the sources are much larger in total angular extent, and we expect much of their diffuse structure to be resolved out. As noted in Section 5.3, we will need to combine existing VLA data in at least some cases in order to sample intermediate scales.

For all of our targets, we are interested not only in the intrinsic (zero-wavelength) linear polarization, which is determined by the magnetic-field geometry, but also the Faraday rotation measure. Typical RM's for our sources are in the range  $10 - 200 \text{ rad m}^{-2}$ , except for M 87 and Cygnus A, which are in cooling core clusters and have RM's up to  $10^4 \text{ rad m}^{-2}$ . The position-angle rotation across the band is  $24(\text{RM}/100 \text{ rad m}^{-2}) \text{ deg}$  at C-band and  $102(\text{RM}/100 \text{ rad m}^{-2}) \text{ deg}$  at L-band. With 512 spectral channels across the band, depolarization within a single channel is not a serious issue.

#### 3.2 FRI jets: L-band imaging

We have selected the 8 twin-jet sources from the LRL sample whose surface-brightnesses allow us to image the jets in detail at L-band (none is bright enough for C-band imaging).<sup>2</sup> These include three sources for which we have published detailed models based on VLA imaging (3C 31, NGC 315 and 3C 296). The sources include a representative range of morphological types, including large-scale structures with plumes (e.g 3C 31) and lobes (e.g. 3C 296), together with the brightest examples of narrow-angle tail (3C 83.1B) and bent-double (3C 465) sources. Our aim is also to include a range of source orientations, from close to the plane of the sky (3C 449) to nearly pole-on. For this reason, we have added one source not in the LRL sample: 3C 371, a nearby BL Lac object, whose radio structure suggests that it is an end-on counterpart of the other sources.

**Total: 9 tracks (154 hr) at L-band.**

#### 3.3 M 87 proper motions

M 87 is the unique example (in the Northern sky) of a radio galaxy which is very close and has high-brightness

---

<sup>2</sup>NGC 315 is now included in the sample on the basis of improved low-frequency flux densities.

structure in its jet, and we propose 5 epochs of observation, separated by roughly 6-month intervals during the Legacy Programme period, in order to measure proper motions. We expect to be able to obtain  $1\sigma$  positional accuracies of between FWHM/80 and FWHM/10 (0.5 – 4 mas) at C-band using cross-correlation techniques (Biretta, Zhou & Owen 1995; Biretta, Sparks & Macchetto 1999). At the distance of M 87, a proper motion of 1 mas/yr corresponds to an apparent velocity of  $0.25c$ . The known velocities in the M 87 jet are typically in the range  $0.5 - 6c$ , so we propose 5 epochs separated by intervals of 6 months over the Legacy Proposal period as a compromise between the time baseline required to study the slower motions in the outer part of the jet and the need to sample motions and variations on smaller scales (knots D and HST-1).

**Total: 5 tracks (65 hr) at C-band and 1 track (13 hr) at L-band.**

### 3.4 Powerful jets

We have selected primarily quasars from the LRL subsample defined by Bridle et al. (1994), whose jets are bright enough to allow imaging with  $\gtrsim 5$  resolution elements across their widths, further restricting the redshift range to  $0.25 \leq z \leq 1$ . No equivalent radio galaxies have bright enough jets, so we have also included Cygnus A, which is comparable in luminosity to the quasars, but anomalously close (and also part of the hot-spots sample). As noted earlier, it is essential for us to observe the end-on counterparts of the 3CR quasars, so we have selected the two clearest examples from LRL (3C 345 and 454.3) together with 3C 273, which is also anomalously close (allowing us to observe the jet in great detail), but only excluded from the LRL sample by the Southern declination limit. The typical spreading rates of the jets are FWHM/length  $\approx 0.05$  (Bridle et al. 1994), so we have chosen to image at L-band for jets longer than 10 arcsec and C-band for the shorter ones.

We note that the dynamic range required to image the three most extreme sources in the sample (3C 273, 345 and 454.3) is extremely challenging and may require special techniques (Section 5.3).

**Total: 5 tracks (76 hr) at L-band + 6 tracks (88 hr) at C-band, excluding one source in common with the hot-spot sample.**

### 3.5 Hot-spots

We have selected the sources with the highest 5-GHz hot-spot flux densities from the compilation of data on the  $z < 1.0$  LRL FR II radio galaxies by Mullin et al. (2008). We then excluded giant sources (which would require multiple pointings to fit in the MERLIN field of view, and which in any case typically do not have existing high-resolution observations), very small sources (where

the data currently cannot distinguish between hot-spots and lobes) and sources without good *Chandra* or optical observations (we do not require a *detection* at optical or X-ray wavelengths, just deep enough observations to provide constraints on the broad-band hot-spot spectrum). We also include the well-studied multiple-hot-spot system Cygnus A (see Section 2.3.1). The sample size is chosen to be large enough to cover the range of observed hot-spot structures, and includes sources with claimed inverse-Compton detections and objects with optical and/or X-ray synchrotron emission, including some well-known cases where the radio and X-ray peaks are offset (e.g. 3C 351, 3C390.3).

**Total: 7 tracks (147 hr) at L-band + 9 tracks (186 hr) at C-band.**

## 4 Complementary projects with *e*-MERLIN and other telescopes

### 4.1 Other Legacy proposals

Our proposal is complementary to all other proposals that make use of radio-loud AGN, for example as tracers of cosmic structure or for their effects on galaxy formation and evolution. This includes, to a greater or lesser extent, the projects described in the LoI's led by Priddey, Muxlow, Simpson, Lal and Edge. An understanding of the energy transport and particle acceleration processes in radio-loud AGN is a crucial step in the chain linking observations (luminosities, number counts) of a population of radio sources to physical quantities of interest such as kinetic luminosity or energy input into the IGM. However, with the exception of the rather specialized project of Lal (which does not conflict with our proposal, since there are no X-shaped sources in our sample) our project is the only proposed legacy study of radio-loud AGN as an end in themselves. With the exceptions of M87 and Cygnus A, where we focus on the high-brightness jets and hot-spots, our sample does not include central galaxies from cooling-core clusters, so there should be little direct overlap with the project on feedback by Edge.

### 4.2 Existing datasets

Our sample selection ensures that there is a wide range of existing multiwavelength data on our targets.

#### 4.2.1 VLA

All our targets have been extensively observed with the VLA, either in single-object studies or as part of attempts to obtain uniform-quality radio imaging of the LRL sample (e.g. Hardcastle et al. 1997; Gilbert et al. 2004; Mullin et al. 2006). The VLA imaging allows us to choose 'representative' small samples for this proposal with some confidence that we do indeed know the range of structures seen in the population as a whole. In principle it will also be possible to use VLA data at appropriate frequencies to constrain the short baselines in our *e*-MERLIN observations, although in practice this will depend on the availability of suitable imaging algorithms (see below).

#### 4.2.2 *HST* and *Spitzer*

The vast majority of the LRL sample, including all our targets, have been studied with the *HST* in the IR, optical and UV as part of various snapshot surveys (e.g. de Koff et al. 1996). In addition, many of our targets are well-known objects and have been studied with longer observations and a wider range of filters. The *HST* data provide important information about the host galaxies and environments of our targets, and also in some cases give con-

straints on optical synchrotron or inverse-Compton emission with a resolution that is well matched to MERLIN's. Although many data already exist, we do not rule out proposing new *HST* observations where appropriate to follow up our *e*-MERLIN results. Almost all of our targets also have good *Spitzer* data.

#### 4.2.3 *Chandra* and *XMM-Newton*

The LRL sample has been well studied with *Chandra* and the vast majority of our targets already have deep *Chandra* data, much of it as a result of observations led by the proposers. We have recently been awarded time for a *Chandra* large project that will complete observations of the  $z < 0.1$  LRL sources (PI Birkinshaw). *Chandra* observations, with  $\sim 0.5$  arcsec resolution, give us our best tracer of high-energy particle acceleration in jets and hot-spots, and also provide the measurements of the small-scale pressure gradient required for jet modelling. *XMM-Newton* observations, which probe the large-scale environments of our targets and are also sensitive to inverse-Compton emission from the radio lobes, exist for a smaller fraction of the sources, but we do have deep *XMM* data for all of the nearby FRI targets, again largely as a result of observations led by members of the team.

### 4.3 EVLA and ALMA proposals

The EVLA will be highly complementary to *e*-MERLIN for our purposes in two ways. Firstly, the EVLA will provide short baselines at matched frequencies (L-band and C-band) and will thus allow us to map the large-scale source structure with the resolution of *e*-MERLIN, the sensitivity to extended structure of the smaller VLA configurations, and the capability of spectral and polarization (e.g. rotation measure) synthesis common to the two instruments; this opens up new possibilities for the discovery of faint compact structure in total intensity and polarization. Secondly, at high frequencies the VLA's resolution starts to become comparable to MERLIN's, while the greatly enhanced sensitivity of the EVLA means that operating at these high frequencies will no longer be prohibitive in terms of observing time for faint features; we will therefore be able to use the EVLA to provide high-frequency counterparts to our high-resolution MERLIN spatial/spectral imaging. We emphasise, however, that the projects we propose here do not *require* EVLA time. Important results will come out of the *e*-MERLIN observations even in the extremely unlikely event that the EVLA does not observe any of our proposed targets.

ALMA will also provide observations at comparable spatial resolution in the mm band, giving much better definition of spectral energy distributions for compact jets and hot-spots, but subject to limited overlap in sky coverage with *e*-MERLIN.

## 5 Software requirements, pipeline processing and data archiving

### 5.1 Pipeline processing

We anticipate that initial calibration of the data will be done at JBCA, but that imaging and further analysis will take place at our home institutes (we require some custom software, as summarized in Section 5.3).

### 5.2 Data products and archiving

We propose to provide reduced data-products and associated documentation to the e-MERLIN project in a format to be agreed (FITS or equivalent). These will include:

1. Final images in Stokes  $I$ ,  $Q$  and  $U$  at a fiducial frequency in the band and at a variety of resolutions.
2. Associated images quantifying variations with frequency across the band, such as spectral index, rotation measure and polarization gradient or their generalizations.
3. Fully self-calibrated uv datasets.
4. Images from other instruments (or links to them) and multifrequency combinations.
5. The results of modelling, in the form of images and animations.

We will also provide the full reduction history and meta-data for ingestion into the VO.

We are happy to abide by the 12-month proprietary period.

### 5.3 Algorithms

Our programme depends critically on the availability of effective algorithms for wide-band synthesis (combined with self-calibration) for a heterogeneous array. We are aware of the work carried out at JBCA on generalizations of the Sault et al. MFS algorithm (e.g. Sault & Conway 1999) and will use this as a starting point. Our project also requires the ability to image over a wide band in linear polarization. A simple method of doing this would be to split the dataset into narrow channels and to use the technique of RM synthesis (Brentjens & de Bruyn 2005), but this is unlikely to deliver the optimum results for low  $s/n$  data. Within our group, Cotton is working on a generalized MFS algorithm using a polynomial in  $\ln \nu$  for the Stokes  $I$  spectrum, but this will not work for polarization. Adding an RM term or using a Fourier series in frequency are possible alternatives. In addition, we will clearly need to remove outlying confusing sources accurately (at least at L-band), although our scientific objectives do not usually require us to image a large fraction of the primary beam.

Until EVLA observations become available (see below), we will need to combine e-MERLIN and VLA data taken with very different spectral configurations (the VLA observations are in continuum mode with bandwidth  $\lesssim 100$  MHz). We will probably develop a variant of the *feathering* technique already implemented in OBIT for this application.

Our targets are all bright, and typically require self-calibration. In most cases this should be straightforward: the brightness distributions tend to be dominated by point-like cores or bright hot-spots at e-MERLIN resolutions). In a few special cases, we will require extremely high dynamic range, and may need to correct for closure errors. We cannot yet assess whether existing routines (e.g. BLCAL) will be effective.

We also note that our requirement for high image fidelity will require use of deconvolution algorithms more sophisticated than standard CLEAN. We have experience in the use of multi-scale clean (in its AIPS and CASA variants) and maximum entropy, and will experiment with the application of these technique to e-MERLIN data.

All of the data-reduction software developed for this project will be freely available as part of the OBIT and CASA package distributions.

### 5.4 Computing hardware

Our estimates are that the data reduction for this project can be carried out on a modest cluster or even a small number of high-end work-stations. Several of the institutes involved in the proposal will have access to the resources required over the duration of the Legacy Proposal period.

## 6 Management and Resource Plan

The programme as a whole will be managed by Laing and Hardcastle. We have divided it into three observational projects, each led by one of the team:

1. low-luminosity jets (Laing);
2. high-luminosity jets (Bridle);
3. hot-spots (Hardcastle);

and two more general activities:

4. rotation-measure analysis (Gabuzda);
5. algorithm development (Cotton).

The division of interests between institutes is given in the table below.

Institute	Work Package	Staff	Notes
Astron	1	Morganti	
Bologna	1	Parma, at least one PhD student	
Bristol	1,2,3	Birkinshaw, Worrall, one or more STFC-funded PhD students	
Cambridge	3,4,5	Alexander, Riley, STFC PDRAs (under review) One or more PhD students	a
Cork	4	Gabuzda, PhD students	
ESO	1,2,4,5	Laing, Guidetti, CASA developer IMPRS student(s)	b,c
Harvard CfA	1,3	Evans	
Hertfordshire	1,2,3	Hardcastle, Croston, STFC PDRA (under review) PhD students	
Manchester	1,2	Garrington, Browne, Leahy PhD student	
NRAO	2, 4	Bridle, Cotton, student support available	d
Oxford	2	Dulwich	

### Notes

- a. Includes development of polarization algorithms in synergy with work funded by the SKA project.
- b. Developer effort will be available to port algorithms to CASA, funded through Radionet FP7 and (if relevant) the ALMA project.
- c. The ESO studentship programme can also provide support for students from other institutes to work with Laing at Garching for periods of 1 – 2 years.
- d. Student support available for algorithm work which is directly relevant to EVLA.

After initial calibration at JBCA, datasets will be distributed amongst the participants in projects 1 – 3 for self-calibration, imaging and reduction to final data products, supported by project 4. Those datasets suitable for rotation-measure analysis will then be passed to project 5. All of the sub-project leaders have many years' experience in reduction, analysis and interpretation of radio synthesis data and have excellent links to the theoretical and modelling communities. The team has access to the necessary computing resources and adequate support for travel to JBCA and project meetings. Our philosophy for algorithm development is to develop software in Cotton's OBIT package, which is inter-operable with AIPS, and to port applications to CASA as they become mature (resources are available within NRAO and ESO for this purpose, at least insofar as they benefit the EVLA and ALMA user communities). A number of image-analysis tools have been developed by members of the team or at their home institutes, including code for jet-modelling (Laing, Bridle), statistical analysis of rotation measure and depolarization (Laing, Guidetti), analysis of inverse Compton X-ray emission (Hardcastle). These are all directly applicable to the present proposal.

## 7 Legacy status

There are three aspects to our decision to ask for legacy status for this project.

The first is scientific. As we have described above, we aim to make significant progress in a number of outstanding areas in the physics of radio-loud AGN. This will be crucial to define the parameters for subsequent work with *e*-MERLIN through the regular time allocation process. For many other legacy projects, the improvement provided by *e*-MERLIN is simply one of sensitivity; we, on the other hand, will be doing science that is *qualitatively* different from anything that has been possible before. By carrying out this work as a legacy project we ensure that the new capabilities of *e*-MERLIN produce scientific results in a timely and efficient manner. We recognise that, since our proposal consists of observations of small samples of objects, it would be perfectly possible to break it up and propose it in the standard way, doubtless in practice spread over several years. However, this would inevitably mean much duplication of effort, much unnecessary competition, and a much longer wait before a scientific consensus could even possibly begin to emerge. Our approach guarantees that, even if we do not know all the answers as a result of our proposed observations, we and the rest of the community will have a much clearer idea of what questions to ask, and how *e*-MERLIN can answer them, by the time the legacy project is complete. (This is particularly important in view of the uncertainties surrounding the long-term funding of *e*-MERLIN at present.)

The second, related aspect concerns the development of new techniques. As our targets are bright, resolved, highly polarized structures with complex, frequency-dependent structure in all Stokes parameters, they represent both the greatest challenge and the greatest technical opportunity for the imaging capabilities of *e*-MERLIN. As discussed above, technical innovation will be needed to exploit *e*-MERLIN imaging to the fullest extent and to achieve all the scientific goals of this project. Here, again, the choice to carry this out as a legacy project will greatly increase efficiency: we will have the resources (in conjunction with the work that is already going on in this area) and the large number of datasets necessary to find a general solution to the imaging problem and to provide it to the community. This aspect of the project's legacy is vital if *e*-MERLIN is to be used effectively for radio-loud AGN work in future. We note, in passing, that the high-quality images we will produce will provide an excellent way of advertising *e*-MERLIN's capabilities to the world-wide scientific community and the general public.

Finally, the third aspect concerns our choice of targets. We plan to observe the brightest and closest representatives of well-defined classes of object, selected from complete samples. The main parent sample (3CRR or

LRL; Laing, Riley & Longair 1983) is flux-limited at the low selection frequency of 178 MHz, thereby minimising orientation bias, and has been checked carefully for selection biases. It has complete identification and redshift information. A wealth of data is available on all the sample members at other wavebands, as discussed above. The present proposal has well-defined scientific aims, so does not attempt to include every type of source represented in the LRL sample, but these facts about the sample mean that the LRL radio galaxies we have chosen to observe (together with the few objects from outside LRL that we include, which are only excluded from LRL on the basis of Galactic latitude or declination, and which include well-known objects such as Cygnus A and 3C 273) are among the best-studied of all radio-loud AGN. Consequently our results — consisting of consistently reduced, fully calibrated data and images, as described above — will be of interest to a very wide community who will make use of them for purposes well beyond our own scientific goals as set out in the current proposal. We can confidently expect that they will be used as a resource by others for many years to come.

## REFERENCES

- Abraham, J., et al. (for the Pierre Auger Collaboration), 2007, *Sci*, 318, 938
- Amato, E., Arons, J., 2006, *ApJ*, 653, 325
- Biretta, J.A., Zhou, F., Owen, F.N., 1995, *ApJ*, 447, 582
- Biretta, J.A., Sparks, W.B., Macchetto, F., 1999, *ApJ*, 520, 621
- Brentjens, M.A., de Bruyn, A.G., 2005, *A&A*, 441, 1217
- Bridle, A.H., Hough, D.H., Lonsdale, C.J., Burns, J.O., Laing, R.A., 1994, *AJ*, 108, 766
- Browne, I.W.A., Clark, R.R., Moore, P.K., Muxlow, T.W.B., Wilkinson, P.N., Cohen, M.H., Porcas, R.W., 1982, *Nature*, 299, 788
- Carilli, C.L., Perley, R.A., Dreher, J.W., Leahy, J.P., 1991, *ApJ*, 383, 554
- Celotti, A., Ghisellini, G., Chiaberge, M., 2001, *MNRAS*, 321, L1
- Cheung, C.C., Harris, D.E., Stawarz, Ł., 2007, *ApJ*, 663, L65
- Dreher, J.W., 1981, *AJ*, 86, 833
- Erlund, M.C., Fabian, A.C., Blundell, K.M., Moss, C., Ballantyne, D.R., 2007, *MNRAS*, 379, 498
- Fanaroff, B.L., Riley, J.M., 1974, *MNRAS*, 167, 31P
- Floyd, D.J.E., et al., 2006, *ApJ*, 643, 660
- Gilbert, G.M., Riley, J.M., Hardcastle, M.J., Croston, J.H., Pooley, G.G., Alexander, P., 2004, *MNRAS*, 351, 845
- Hardcastle, M.J., 2006, *MNRAS*, 366, 1465
- Hardcastle, M.J., Alexander, P., Pooley, G.G., Riley, J.M., 1996, *MNRAS*, 278, 273
- Hardcastle, M.J., Alexander, P., Pooley, G.G., Riley, J.M., 1997, *MNRAS*, 288, 859
- Hardcastle, M.J., Birkinshaw, M., Cameron, R.A., Harris, D.E., Looney, L.W., Worrall, D.M., 2002, *ApJ*, 581, 948
- Hardcastle, M.J., Croston, J.H., Kraft, R.P., 2007, *ApJ*, 669, 893
- Hardcastle, M.J., Sakelliou, I., 2004, *MNRAS*, 349, 560
- Hardcastle, M.J., Worrall, D.M., Kraft, R.P., Forman, W.R., Jones, C., Murray, S.S., 2003, *ApJ*, 593, 169
- Harris, D.E., Carilli C.L., Perley, R.A., 1994, *Nat*, 367, 713
- Heavens, A.F., Meisenheimer, K., 1987, *MNRAS*, 225, 335
- Hillas, A.M., 1984, *ARA&A*, 22, 425
- Jester, S., Röser, H.-J., Meisenheimer, K., Perley, R., 2005, *A&A*, 431, 477
- de Koff, S., et al., 1996, *ApJS*, 107, 621
- Kraft, R.P., Birkinshaw, M., Hardcastle, M.J., Evans, D.A., Croston, J.H., Worrall, D.M., Murray, S.S., 2007, *ApJ*, 659, 1008
- Laing, R.A., 1982, in *Extragalactic Radio Sources*, eds Heeschen D.S., Wade C.M., IAU Symp. 97, Kluwer, Dordrecht, p. 161
- Laing, R.A., 1993, in Burgarella, D., Livio, M., O’Dea, C.P., eds, *Space Telescope Sci. Inst. Symp. 6: Astrophysical Jets*. Cambridge University Press, Cambridge, p. 95
- Laing, R.A., Bridle, A.H., 2002a, *MNRAS*, 336, 328
- Laing, R.A., Bridle, A.H., 2002b, *MNRAS*, 336, 1161
- Laing, R.A., Bridle, A.H., Parma, P., Feretti, L., Giovannini, G., Murgia, M. and Perley, R.A., 2008, *MNRAS*, 386, 657
- Laing, R.A., Canvin, J.R., Cotton, W.D., Bridle, A.H., 2006a, *MNRAS*, 368, 48
- Laing, R.A., Canvin, J.R., Bridle, A.H., Hardcastle, M.J., 2006b, *MNRAS*, 372, 510
- Laing, R.A., Riley, J.M., Longair, M.S., 1983, *MNRAS*, 204, 151
- Lara, L., Giovannini, G., Cotton, W.D., Feretti, L., Venturi, T., 2004, *A&A*, 415, 905
- Leahy, J.P., Perley, R.A., 1991, *AJ*, 102, 537
- Leahy, J.P., Perley, R.A., 1995, *MNRAS*, 277, 1097
- Ledlow, M.J., Owen, F.N., 1996, *AJ*, 112, 9
- Marshall, H.L., Miller, B.P., Davis, D.S., Perlman, E.S., Wise, M., Canizares, C.R., Harris, D.E., 2002, *ApJ*, 564, 683
- Meisenheimer, K., Röser, H.-J., Hiltner, P.R., Yates, M.G., Longair, M.S., Chini, R., Perley, R. A., 1989, *A&A*, 219, 63
- Mullin, L.M., Hardcastle, M.J., Riley, J.M., 2006, *MNRAS*, 372, 113
- Mullin, L.M., Riley, J.M., Hardcastle, M.J., 2008, *MNRAS* in press.
- O’Dea, C.P., Owen, F.N., 1986, *ApJ*, 301, 841
- Sambruna, R.M., Donato, D., Tavecchio, F., Maraschi, L., Cheung, C.C., Urry, C.M., 2007, *ApJ*, 670, 74
- Sault, R.J., Conway, J.E., 1999, in G.B. Taylor, C.L. Carilli, R.A. Perley, eds, *Synthesis Imaging in Radio Astronomy II*, ASP Conference Series, 180, 419
- Swain, M.R., Bridle, A.H., Baum, S.A., 1998, *ApJ*, 507, L29
- Tavecchio, F., Maraschi, L., Sambruna, R.M., Urry, C.M., 2000, *ApJ*, 544, L23
- Tavecchio, F., Cerutti, R., Maraschi, L., Sambruna, R.M., Gambill, J.K., Cheung, C.C., Urry, C.M., 2005, *ApJ*, 630, 721
- Tregillis, I.L., Jones, T.W., Ryu, D., Park, C., 2002, *NewAR*, 46, 387
- Uchiyama, Y., et al., 2006, *ApJ*, 648, 910
- Wardle, J.F.C., Aaron, S.E., 1997, *MNRAS*, 286, 425
- Worrall, D.M., Birkinshaw, M., Laing, R.A., Cotton, W.D., Bridle, A.H., 2007, *MNRAS*, 380, 2

## A Source list

Name	IAU <sup>a</sup> (J2000)	$z$	$\nu^b$	Time <sup>c</sup> hr	$S_{\text{tot}}^d$ Jy	$S_{\text{core}}$ mJy	$S_{\text{max}}^e$ $\mu\text{Jy} / \text{beam}$	$S_{\text{min}}^f$	$\theta^g$ asec	Reference
Sample 1: FRI jets										
NGC 315	0057+30	0.0165	L	17	~4	400	240	60	30	Laing et al. (2006a)
3C 31	0107+32	0.0169	L	17	5.4	74	950	75	20	Laing et al. (2008)
3C 66B	0223+42	0.0213	L	22	9.4	180	4200	100	20	Hardcastle et al. (1996)
3C 83.1B	0318+41	0.0251	L	21	8.9	12	240	50	30	O’Dea & Owen (1986)
3C 264	1145+19	0.0217	L	14	5.9	225	15500	80	10	Lara et al. (2004)
3C 272.1	1225+12	0.0035	L	13	6.5	130	1600	90	40	Laing & Bridle (in prep.)
M87 (3C 274)	1230+12	0.0044	L	13	220	4000	600	100	60	Biretta, Zhou & Owen (1995)
			C	$5 \times 13$	72	4000	130	20	20	
3C 296	1416+10	0.0247	L	12	4.2	53	420	55	20	Laing et al. (2006b)
3C 371	1806+69	0.0510	L	24	2.5	2500	15500	80	30	Sambruna et al. (2007)
3C 465	2338+27	0.0302	L	16	7.8	210	55	20	45	Hardcastle & Sakelliou (2004)
Sample 2: Powerful jets										
3C 133 <sup>j</sup>	0502+25	0.2775	C	15	2.15	230	320	80	5	Floyd et al. (2006)
3C 175	0713+11	0.768	L	13	2.44	24	360	90	28	Bridle et al. (1994)
3C 207	0840+13	0.684	C	13	1.43	540	360	90	7	Mullin et al. (2006)
3C 263	1137+66	0.6563	L	24	3.11	160	640	160	16	Bridle et al. (1994)
3C 273 <sup>h</sup>	1229+02	0.158	L*	11	32.0	32000	$2 \times 10^5$	1700	22	Jester et al. (2005)
			C*	11	30.0	30000	7000	60	22	
3C 275.1	1243+16	0.557	L	14	2.95	210	1440	360	8	Gilbert et al. (2004)
3C 334	1620+17	0.555	L	14	2.15	110	1200	300	17	Bridle et al. (1994)
3C 345 <sup>h</sup>	1642+39	0.594	C	20	8600	7.8	420	80	3	Browne et al. (1982)
3C 336	1624+23	0.927	C	15	0.69	20	120	30	7	Bridle et al. (1994)
Cygnus A <sup>i</sup> (3C 405)	1957+41	0.0565	L*	21	1586	500	10000	100	50	Carilli et al. (1991)
			C*	21	363	776	300	20	50	
3C 454.3 <sup>h</sup>	2253+16	0.859	C	14	12000	10000	280	55	5	Browne et al. (1982)
Sample 3: Hot-spots										
3C 20	0040+52	0.174	C	24	5.2	2.6	4500	20	4	Hardcastle et al. (1997)
			L	24	12.0	< 1.0	$10^5$	300	8	
3C 33	0106+13	0.0595	C	13	4.7	24	1200	10	6	Leahy & Perley (1991)
			L	13	12.4	50	36000	50	14	
3C 47	0133+21	0.425	C	15	1.1	74	800	10	4	Bridle et al. (1994)
3C 123	0433+30	0.2177	C	17	19.9	100	18000	300	2	Hardcastle et al. (1997)
			L*	17	48.6	64	$5 \times 10^5$	10000	2	
3C 263	1137+66	0.6563	C	24	1.1	157	10000	10	2	Hardcastle et al. (2002)
3C 295	1409+52	0.4614	C	24	11.1	3	40000	400	5	Gilbert et al. (2004)
3C 303	1441+52	0.141	L*	24	2.4	125	10000	200	5	Leahy & Perley (1991)
3C 351	1704+61	0.371	C	24	1.3	6.5	8500	50	7	Gilbert et al. (2004)
			L*	24	3.3	< 36	$2 \times 10^5$	500	7	
3C 390.3	1845+80	0.0569	C	24	4.2	330	200	10	7	Leahy & Perley (1995)
			L	24	11.2	233	5000	100	20	
Cygnus A (3C 405)	1957+41	0.0565	C*	21	363	776	18000	200	10	Carilli et al. (1991)
			L*	21	1586	500	$5 \times 10^5$	5000	10	

## Notes

- a. Sources will be observed with the phase centre at the positions of the radio cores, which are all known to sub-arcsecond accuracy. The IAU names are given here purely as an indication for scheduling purposes.
- b.  $\nu$  denotes the observing band (L or C). An asterisk indicates that we could use MkII in place of the Lovell Telescope without serious degradation of the results.
- c. The proposed track lengths are for all telescopes in the array to have elevations  $> 5^\circ$ .
- d. All flux densities are quoted for the observing band in question.
- e.  $S_{\max}$  is the expected peak surface brightness in the region of interest (excluding the core) at e-MERLIN resolution. We assume beamwidths of 0.15 arcsec and 0.04 arcsec FWHM at L and C bands, respectively.  $S_{\max}$  has been computed using the best available images, assuming that the sources have  $\alpha = 0.6$  (a good approximation for jets and hot-spots). We make the conservative assumption that the emission is fully resolved.
- f.  $S_{\min}$  is the minimum surface brightness we are attempting to observe, computed as for  $S_{\max}$ .
- g. The scale quoted is the area over which we expect detect significant flux at e-MERLIN resolutions: the largest angular sizes of the sources are in most cases much larger.
- h. The total and core flux densities for 3C 273, 345 and 454.3 are not contemporaneous.
- i. The observations for 405 are in common between samples 2 and 3.
- j. 3C 133 is very slightly outside the Galactic latitude limit of the LRL sample, but otherwise satisfies the selection criteria.